WPJET3-PR(18) 20499

L W Packer et al.

Activation of ITER materials in JET: nuclear characterisation experiments for the long-term irradiation station

Preprint of Paper to be submitted for publication in
Nuclear Fusion

This work has been carried out within the framework of the EUROfusion Consortium and has received funding from the Euratom research and training programme 2014-2018 under grant agreement No 633053. The views and opinions expressed herein do not necessarily reflect those of the European Commission.

Activation of ITER materials in JET: nuclear characterisation experiments for the long-term irradiation station

L. W. Packer[a,1], P. Batistoni[b], S. C. Bradnam[a], B. Colling[a], S. Conroy[c], Z. Ghani[a], M. R. Gilbert[a], S. Jednorog[e], E. Łaszyńska[e], D. Leichtle[f], I. Lengar[g], J.W.Mietelski[d], R. Misiak[d], C.R.Nobs[a], M. Pillon[b], S. Popovichev[a], V. Radulović[g], I.E. Stamatelatos[h], T. Vasilopoulou[h], A. Wójcik-Gargula[d], and JET Contributors[2]

[a] *Culham Centre for Fusion Energy, Culham Science Centre, Abingdon, Oxon, OX14 3DB, UK*
[b] *ENEA - Department of Fusion and Technology for Nuclear Safety and Security via E. Fermi 45, 00044 Frascati (Rome), Italy*
[c] *VR Association, Uppsala University, Department of Physics and Astronomy, PO Box 516, SE-75120 Uppsala, Sweden*
[d] *Institute of Nuclear Physics, Polish Academy of Sciences, PL-31-342 Krakow, Poland*
[e] *Institute of Plasma Physics and Laser Microfusion, 01-497 Warsaw, Poland*
[f] *Fusion for Energy, Josep Pla 2, Torres Diagonal Litoral B3, 08019 Barcelona, Spain*
[g] *Reactor Physics Department, Jožef Stefan Institute, Jamova cesta 39, SI-1000 Ljubljana, Slovenia*
[h] *Institute of Nuclear and Radiological Sciences, Technology, Energy and Safety, NCSR Demokritos, Athens, 15310, Greece*

Abstract

This paper details progress in experimental characterisation work at JET for the long-term irradiation station, conducted as part of a project to perform activation experiments using ITER materials. The aim is to take advantage of the significant 14 MeV neutron yield expected during JET operations to irradiate samples of materials that will be used in the manufacturing of ITER tokamak components, such as Nb_3Sn, SS316L steels from a range of manufacturers, SS304B, Alloy 660, W, CuCrZr, OF-Cu, XM-19, Al bronze, NbTi and EUROFER. This paper presents an assessment of the nuclear environment at the relevant irradiation locations at JET, measured using a range of high purity dosimetry foils: Ti, Ni, Y, Fe, Co, Sc, and Ta, irradiated with fusion neutrons at

[1] Corresponding author
[2] See the author list of X. Litaudon et al. 2017 Nucl. Fusion 57 102001

JET over a period of 15 months. Experimental results are presented and compared to simulation predictions using a JET MCNP model coupled with the FISPACT-II inventory code. Comparisons are made for a total of 11 nuclear reactions using a range of nuclear data libraries in calculations.

Keywords: activation, neutronics, fusion

1. Introduction

The planned high profile experiments over the next few years at the Joint European Torus (JET), notably including a deuterium-tritium (D–T) experimental phase, are expected to produce large neutron yields of up to 1.7×10^{21} neutrons. The scientific objectives of the campaign are linked with a technology programme [1] with the aim to deliver the maximum scientific and technological return from those operations, with particular emphasis on technology exploitation via the high neutron fluxes predicted in and around the JET machine. Importantly, the programme aims to extract experimental data that is relevant to the international effort to design, construct and operate the International Thermonuclear Experimental Reactor (ITER), the tokamak device being constructed in Cadarache, France, designed to produce significant fusion power of up to 500 MW with corresponding D–T neutron emission rates of 1.77×10^{20} neutrons per second. The range of activities at JET are diverse and significant results have been obtained to date in support of ITER [2]. Nuclear technology related experimental activities under the programme provide an important contribution by giving insight on induced activation and damage to ITER materials, nuclear safety, tritium fuel cycle, nuclear waste characterisation and production levels for example. Nuclear activities performed to date include calibration of neutron yield monitors using a 14 MeV neutron generator [3], neutronics benchmark experiments for neutron streaming and shut-down gamma fields [4, 5, 6, 7, 8], nuclear diagnostics and data processing for tritium breeding blankets [9], and activation measurements with supporting analyses for fusion materials [10, 11]. Data retrieved under the JET experimental program aims to support, develop

and lead to the improvement of radiation transport and activation simulation capabilities for fusion materials via benchmarking and validation in fusion-relevant operational conditions. Such capabilities are important as the underlying methods, tools and data are applied extensively to predict a wide range of nuclear phenomena and impacts associated with components and materials that will be used in ITER operations, and indeed those foreseen in preparing for next-step DEMO concepts.

This paper describes the activities performed to date under a neutron activation sub-project, which has the aim to irradiate a range of real ITER materials in JET experiments and obtain valuable nuclear response benchmark data from those materials. The work covered here includes details of the collaborative work performed in experimental characterisation of the long-term irradiation stations (LTIS) that were used in a 2015–16 JET deuterium-deuterium (D–D) campaign, carried out using a range of high-purity dosimetry foils which were irradiated inside the LTIS assemblies and then disseminated for measurement using high resolution gamma spectrometry systems across four EU laboratories. Activity predictions obtained using neutron transport and activation simulations using an updated JET radiation transport model are tested against experimental activity measurements and are shown to demonstrate a successful and robust simulation approach and predictive capability.

The neutron activation project schedule currently extends to the end of this decade, in step with the overarching JET experimental programme. A D–D campaign is planned for early 2018, followed by a T–T experimental campaign and finally a D–T campaign at the end of the schedule. In each of these phases a selection of real ITER materials, together with a range of dosimetry foils, will be irradiated to enable absolute monitoring of the neutron flux within an irradiation assembly environment. In parallel with the nuclear characterisation efforts discussed here, and following on from previous work [10], progress in acquisition and preparation of ITER materials samples has taken place. A selection of the samples has been collected by Fusion for Energy. These have been shipped to the UK to be prepared into disc samples for JET installation

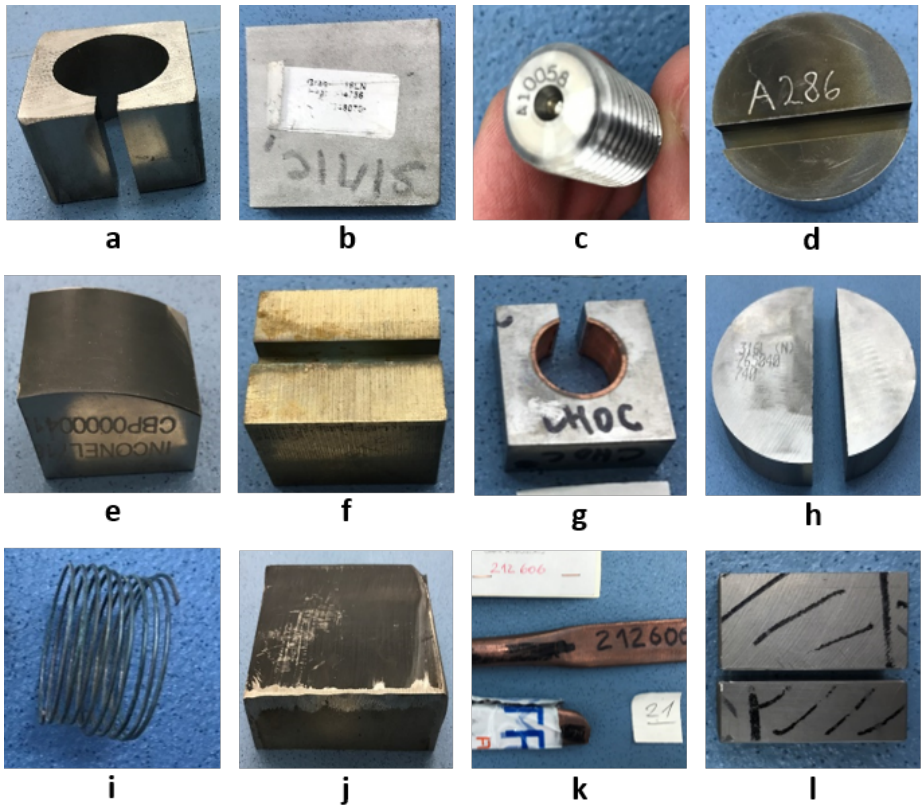

Figure 1: Selected ITER material samples: a) PF coil jacket; b) Radial closure plate for TF coil; c) TF coil case specimen; d) In-wall shielding material; e) Inconel 718; f) Divertor material g) Divertor W monoblock; h); Vacuum vessel forging; i) Reacted TF strand; j) Vacuum vessel plate; k) CuCrZr pipes for the divertor; l) Eurofer 97-3 material.

in 2018. Some examples of the bulk items are shown in figure 1. These include: poloidal field (PF) coil jacket and toroidal field coil radial closure plate steels, EUROFER 97-3 steel, W and CuCrZr materials from the divertor, Inconel 718, CuCrZr and 316L stainless steel for blanket modules, vacuum vessel forging samples and NbSn toroidal field coil strands, for example.

2. JET irradiation assemblies: long term irradiation stations

Dosimetry foil samples were irradiated in JET in two LTIS assemblies during 2015–16 over a 15 month period with 3682 experimental JET deuterium plasma shots. The objective of the exercise was to evaluate the neutron field at the location of these assemblies via measurements of dosimetry foils that were irradiated in this field via activation measurements with results compared with those obtained using detailed neutron transport and activation simulations. The assemblies were manufactured from stainless steel with a tungsten shim to protect the foils from the harsh temperature and radiation fields induced by the plasma environment. Each assembly provided 30 cavities of 18 mm in diameter with a depth of 2 mm, each cavity housing up to 4 dosimetry foils in a stacked arrangement. The assemblies were installed into JET in June 2015 prior to the experimental campaign; one in octant 4 and the other in octant 8. The left-hand side image in figure 2 shows a photo of the octant 8 assembly loaded with dosimetry foils prior to irradiation. The right-hand side image in figure 2 shows a model of the location of the LTIS. The green components positioned to the right of the LTIS assembly are the JET poloidal limiters, which are partially formed of beryllium.

3. Neutron transport and activation simulations

Neutron transport calculations were performed with the Monte Carlo-based radiation transport code MCNP-6.1 [12] with an updated JET MCNP model containing a geometric representation of the long-term irradiation assembly. The purpose of the simulations were to determine via calculation a representative neutron spectra within the assembly, which can be used in subsequent activation calculations to derive activity quantities for the nuclides of interest, with the overall aim of comparing simulated results to activity measurements.

3.1. Description of the LTIS MCNP model

Figure 3 shows images of the JET MCNP geometry containing the LTIS near to the poloidal limiter. The geometry was converted from CAD format

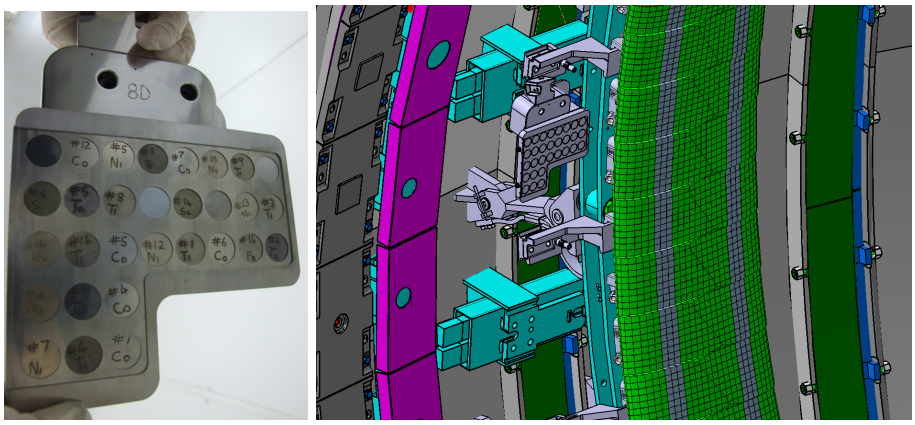

Figure 2: (LHS) Photograph of the 8D LTIS assembly containing dosimetry foils prior to irradiation in 2015; (RHS) CAD image of the location of the LTIS in JET near to a poloidal limiter.

into MCNP geometry using the SuperMC software [13] and from detailed engineering drawings. The activation foil assembly, i.e. the tungsten shim, sample holder tray and box sample holder were modelled in detail, and individual foil cavity locations were modelled explicitly. However, only representative foils were defined in the model i.e. individual foils were not modelled in detail in every location within the assembly. The holder for fixing the assembly to the first wall has been modelled using simplified geometry with small features such as individual screws being removed. The poloidal limiter near to the LTIS contains Be; this was explicitly modelled as it was judged important to accurately predict the low energy component of the neutron spectrum relevant to capture reactions in this location.

3.2. Activation calculations using FISPACT-II

A set of activation calculations were conducted using the FISPACT-II inventory code [14] for the JET operational period in order to predict the dosimetry foil activities as a function of time. This was done using the MCNP calculated neutron spectrum at the LTIS position using the International Reactor Dosimetry and Fusion File, IRDFF-1.05, cross section data as input into the

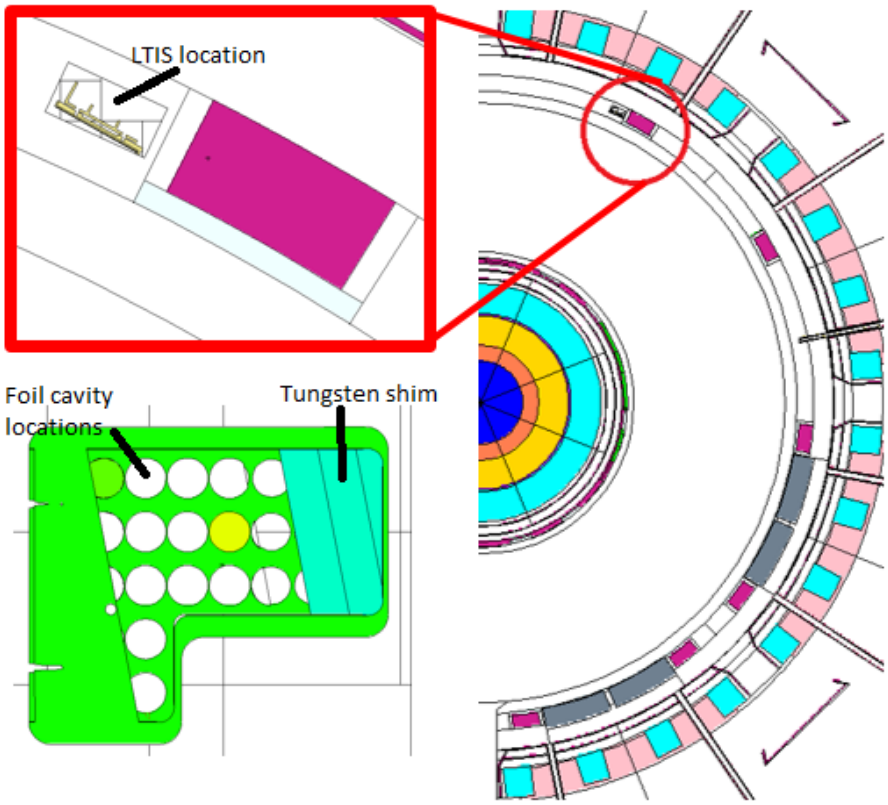

Figure 3: MCNP model x-y slice section of JET showing the location of the octant 8 LTIS assembly (expanded section); left-hand bottom figure shows the LTIS with cutaway section revealing some of the foil cavities.

FISPACT-II code. For one particular reaction the European Activation File, EAF-2010, and the Talys Evaluated Nuclear Data Library, TENDL-2015, cross section data were used in absence of IRDFF-1.05 cross section data. Total neutron yield values per JET plasma shot were recorded from measurements reported by the JET fission chamber diagnostic system and these have been modeled as 1 second square pulses in the irradiation history used in the FISPACT-II calculations. The JET fission chamber diagnostic system, also referred to as the KN1 system, consists of three pairs of ^{235}U and ^{238}U fission chambers. The chambers are mounted on the vertical magnetic limbs located in octants 2, 6, and 8, at a radius of 782 cm in the equatorial plane at the JET facility. They serve to measure the absolute neutron yield and its variation in time, subsequently allowing for the determination of plasma ion temperature and hence the fusion power generated in the tokamak. Each chamber is shielded against gamma rays with 5.5 cm of lead shielding and moderated, using 5 cm of polythene, and with a 1 mm thick Cd thermal neutron filter, to provide a relatively flat energy response for neutrons in the range 1–18 MeV. The fission chambers have been calibrated in-situ with a ^{252}Cf radioisotope source for D–D fusion energies around 2.45 MeV and more recently using a 14 MeV neutron generator in preparation for the future D–T campaign [15]. Using the full dynamic range of both chambers a yield of 10^8–10^{20} n/s can be detected with a time resolution of 10 ms.

Figure 4 shows the predicted activity results obtained from the activation calculations, along with some of the key inputs to the calculation. Figure 4(a) shows the JET neutron yield per pulse over time, as reported by the KN1 system. The foils were installed at JET in June 2015 and irradiated during the JET D–D campaign which ran from the 27th August 2015 until the 15th November 2016; a period of 446 days. During this period, a total yield of 2.26×10^{19} neutrons was delivered in 3682 experimental JET shots. The inset neutron spectrum shown in 4(b) exhibits the two characteristic neutron energy peaks from the D–D and D–T fusion reactions. Although the principal operation mode of JET was in D–D plasma mode in this campaign, principally resulting in the production of

neutrons around 2.45 MeV, the triton produced from one branch of the D–D fusion reaction leads to 14 MeV neutrons being present in the field from D–T reactions, which is reported to be typically 1% in JET according to [16, 17]. This assumed value of 1% has been adopted in our activation calculations.

4. Experimental activities

In total, 176 foils were irradiated in the LTIS in JET octants 4 and 8 throughout the duration of the experimental campaign. Elemental foils including Ti, Ni, Y, Fe, Co, Sc, and Ta were provided by the following institutions; 1) ENEA, 2) NCSRD, 3) IFJPAN and 4) CCFE, with foil thicknesses varying from 0.1 mm to 1 mm, although the majority of the foils that were irradiated had a nominal thickness of 0.5 mm. Following completion of the experimental campaign in late-2016 the foils were retrieved, in January 2017, via a clearance process conducted in the JET beryllium handling facility. This was to determine that the samples were free of Be dust and radiological contamination, ensuring that the foils could be shipped to various laboratories for analyses. Most of the foils were successfully retrieved and distributed back to the originating laboratories for gamma spectrometry analyses. However some of the Ti foils were either partially or completely destroyed during the irradiation. The cause is being investigated, though the H environment, high temperature and radiation effects are key considerations.

4.1. Dosimetry foil nuclear reactions

Table 1 specifies a list of reactions associated with each dosimetry foil type used in these experiments: Co, Fe, Ni, Sc, Ta, Ti and Y. Where there are multiple reaction pathways to the product nuclide the nomenclature (n,x) has been used to indicate the production reaction. The dominant pathway to the product nuclide is also identified for convenience. The principal gamma line(s) observed for the product nuclide is provided in each case.

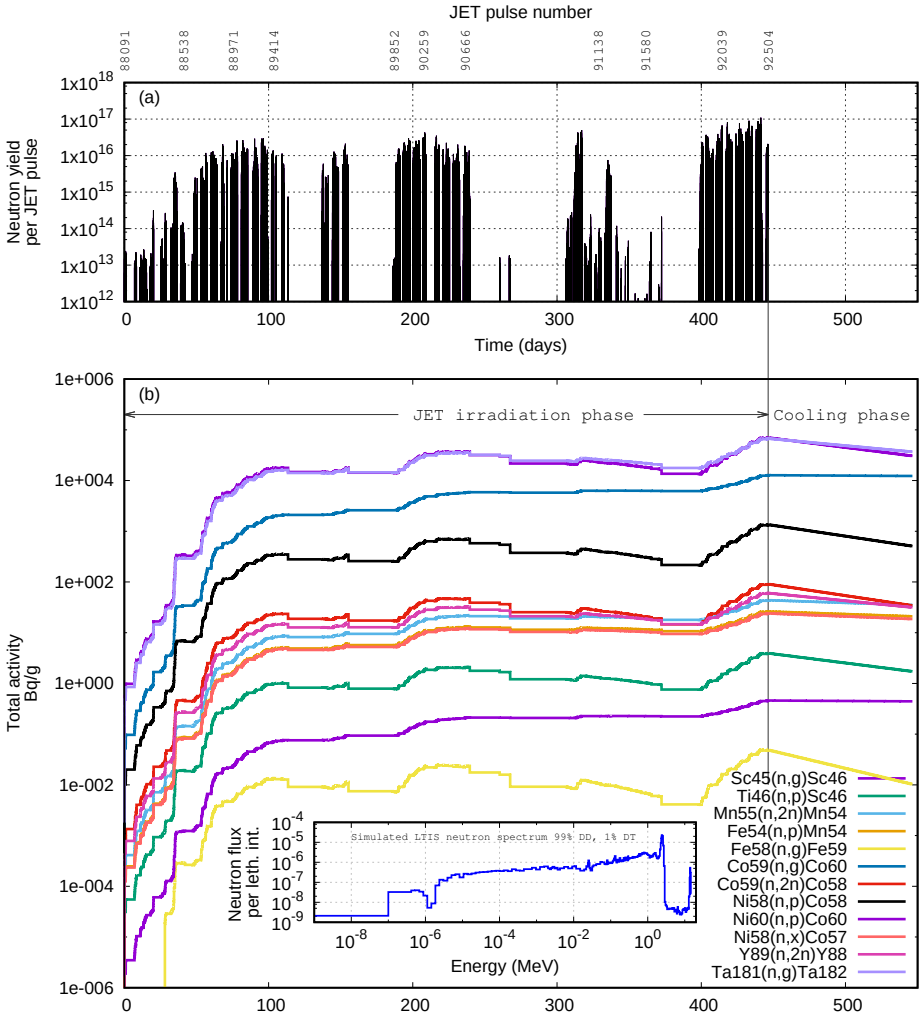

Figure 4: (a) JET neutron yield per pulse between 27/08/2015 and 15/11/2016; (b) Simulated specific activities calculated over time for dosimetry foils located within the long-term irradiation station assembly, exposed to JET experimental campaigns calculated using FISPACT-II.

Table 1: Dosimetry foil types, associated reactions and their principle gamma emission lines.

Foil type	**Reaction type; (dominant pathway)**	**Principle gamma line(s) (keV)** (data from [18] unless otherwise stated)
Co	^{59}Co(n,2n)^{58}Co	810.759
	^{59}Co(n,γ)^{60}Co	1173.228, 1332.492
Fe	^{58}Fe(n,γ)^{59}Fe	1099.245, 1291.590
	^{nat}Fe(n,x)^{54}Mn; (^{54}Fe(n,p)^{54}Mn)	834.838
Ni	^{nat}Ni(n,x)^{58}Co; (^{58}Ni(n,p)^{58}Co)	810.759
	^{nat}Ni(n,x)^{60}Co; (^{60}Ni(n,p)^{60}Co)	1173.228, 1332.492
	^{nat}Ni(n,x)^{57}Co; (^{58}Ni(n,n'p)^{57}Co)	14.41295, 122.061, 136.474
Sc	^{45}Sc(n,γ)^{46}Sc	889.271, 1120.537
Ta	^{181}Ta(n,γ)^{182}Ta	1121.290, 1221.395, 1189.040 [19]
Ti	^{nat}Ti(n,x)^{46}Sc; (^{46}Ti(n,p)^{46}Sc)	889.271, 1120.537
Y	^{89}Y(n,2n)^{88}Y	898.036, 1836.052

4.2. Gamma spectrometry measurements at independent laboratories

Foil activity measurements were carried out at each of the four laboratories with HPGe detectors calibrated using mixed nuclide gamma sources that are traceable to a primary standard. Whilst specific laboratory calibration methodologies were similar, the calibration techniques and analysis software used were different in some cases. Nuclide gamma sources included some from the following range, prepared for or used as a gamma source calibration standard: ^{241}Am, ^{109}Cd, ^{57}Co, ^{51}Cr, ^{85}Sr, ^{54}Mn, ^{133}Ba, ^{137}Co, ^{203}Hg, ^{60}Cs and ^{88}Y. Further measurement correction factors were made by laboratories, where necessary, to account for geometric and dosimetry foil self-attenuation effects; brief details of the different laboratory approaches are provided below.

The NCSRD laboratory measurements were performed using a coaxial germanium detector (GEM80) with 85% relative efficiency, energy resolution, full

width at half maximum (FWHM) of 1.67 keV at the 1332 keV and a peak-to-Compton ratio of 93:1. The detector was surrounded by 5 cm lead shielding for background radiation reduction (see figure 5(a)). Each foil was measured for 1 hour. Co and Ni foils were measured at a source-to-detector distance of 12 cm whilst the Ta foils—due to their much higher activity rates—were counted at a distance of 18 cm. Coincidence summing effects become significant in close geometry measurements and the TrueCoinc package [20] was used to make the necessary corrections.

The ENEA laboratory measurements were carried out using the GammaVision v8.04 spectrometry analysis software and a HPGe detector with aluminium endcap and 60% relative efficiency manufactured by ORTEC. This detector was absolutely calibrated for point and 20 mm disc source geometries at a source–detector distance of 10 cm from the endcap using traceable mixed gamma sources from a CEA metrology laboratory. 34 foils were analysed by ENEA, including thin cobalt (nominally 0.05 mm), iron, nickel, and titanium. Of these, the two titanium foils were less active and were measured as a pair in stack configuration. Two ENEA Co foils were measured at both ENEA and IFJ laboratories (see E1 and E2 data points in figure 14).

At the CCFE laboratory two detectors were used to perform the measurements for Ti, Fe, Co, Ni, Y and Ta; a copper endcap HPGe detector manufactured by Ortec and a Broad Energy Germanium (BEGe) (see figure 5(b)) detector manufactured by Canberra. A close source-to-detector geometry was used for lower activity samples, where the foil is positioned directly on the detector endcap, and a 15 cm source-to-detector distance geometry was used for higher activity samples, where the foil is positioned on a plastic mount above the endcap. Coincidence summing correction factors were calculated using the LabSOCS [21] software package.

The IFJPAN laboratory measurements (see figure 5(c)) were performed using two coaxial HPGe detectors (with a 30% relative efficiency each) of the whole-body spectrometer (WBS) located at a basement-level at IFJPAN. The spectrometer shielding was made of 17 cm thick 19th century steel free from ^{60}Co

traces present in all modern steels. This box-like shield has a size of $1.6 \times 1.5 \times 2.2$ m and a weight of 18 tonnes. All of the inner walls of the steel shielding are covered with a 3 mm copper lining. For the duration of measurements, an additional 5 cm lead shield was mounted between the detectors to eliminate detector cross-talk effects between the two detectors when different samples were measured simultaneously. Spectra were collected using a commercial system and analysed using in-house software developed at IFJPAN. The IFJPAN calibration standards were produced using a mixed gamma solution traceable to the Czech Metrology Institute. Standards were prepared by slow evaporation of the solution onto filter papers with suitable metal shims which were then hermetically sealed in polyvinyl chloride capsules using trichloroethylene. The benefit of this approach is that self-attenuation and geometry factors are inherent in the calibration standard i.e. further calculated correction factors to be applied to the measurements were not necessary.

An example measured spectrum obtained by CCFE from a Ni foil, 'NiCCFE2', following irradiation is shown in figure 6. One can observe the characteristic lines from ^{57}Co, ^{58}Co and ^{60}Co. The non-labelled peaks that are evident in the spectra are the annihilation peak at 511 keV and a true coincidence summation peak induced by an annihilation photon combined with the 810.5 keV ^{58}Co gamma line.

An example spectrum measured by CCFE for a Y foil, 'YCCFE1', is shown in figure 7. Here, one can observe the two characteristic lines from ^{88}Y, along with several lines due to impurities. Although the irradiated samples consisted of high purity (about 99.9%) metal foils, other radionuclides were produced due to the activation of minor impurities present in the samples. These are likely to be from Ta impurities present in the Y, Sc and Ti foils resulting in the observation of Ta-182. The supplier Alfa Aesar reported 170 ppm Ta present in the Sc foils for example, though certificates for Y and Ti were not provided. In addition, Co impurities thought to be present in the Fe and Ti, resulted in the observation of Co-60 and Co-58 lines.

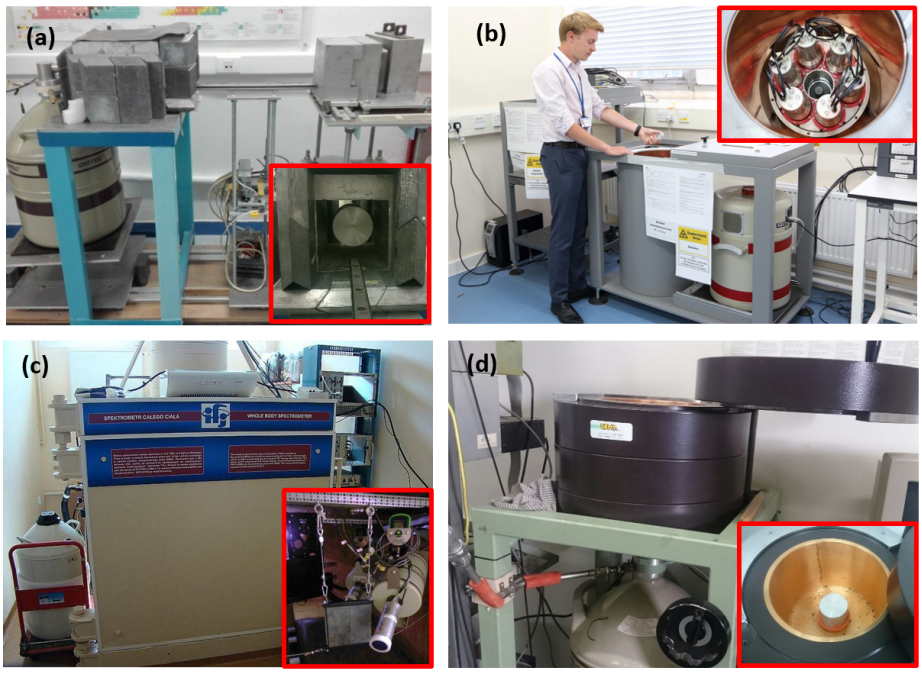

Figure 5: (a) NCSRD 85% relative efficiency HPGe coaxial detector and (inset) detector shown inside low background configuration; (b) CCFE BEGe detector and cryogenic recycler with (inset) NaI Compton suppression ring inside a Pb/Sn/Cu low background shield; (c) Whole-body spectrometer at IFJ PAN view from outside low background shielding, and (inset) a pair of 30% relative efficiency HPGe detectors inside the shielding separated by a suspended lead shield; (d) ENEA HPGe detector inside low background shield.

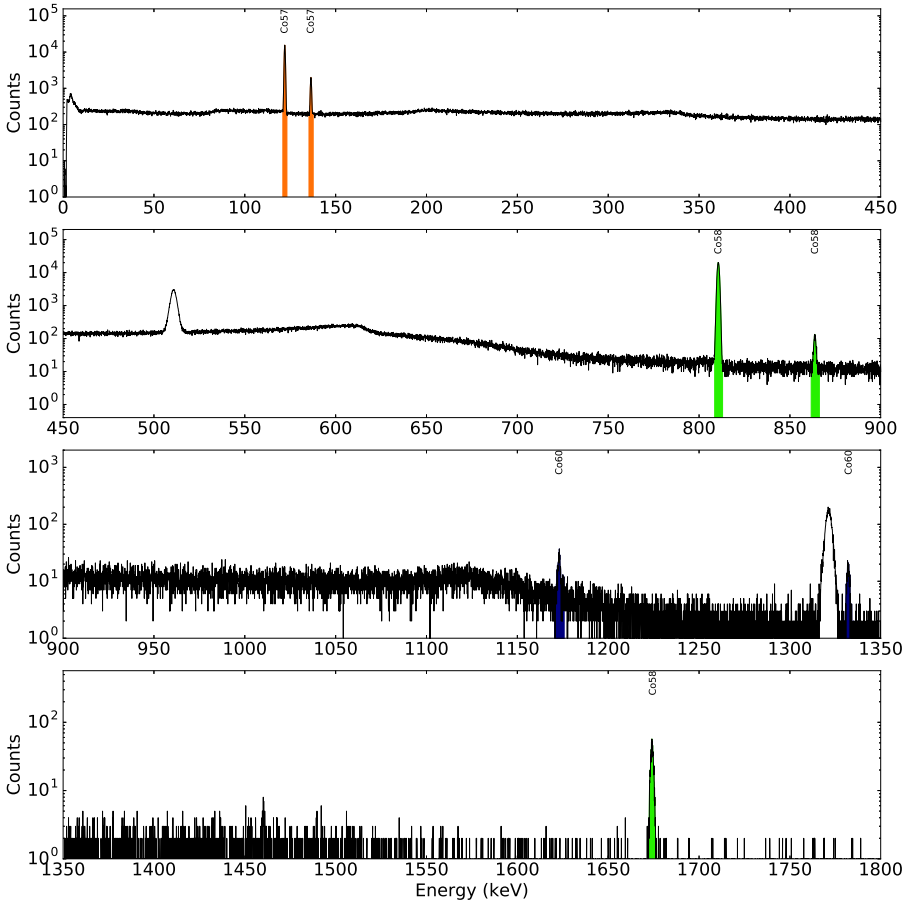

Figure 6: HPGe measurement taken from an Ni foil 'NICCFE2', showing characteristic peaks from ^{57}Co, ^{58}Co and ^{60}Co. The two unmarked peaks are the characteristic annihilation peak at 511 keV, and at approximately 1321.8 keV, a ^{58}Co true coincidence peak for positron annihilation at 511 keV summed with the 810.8 keV emission.

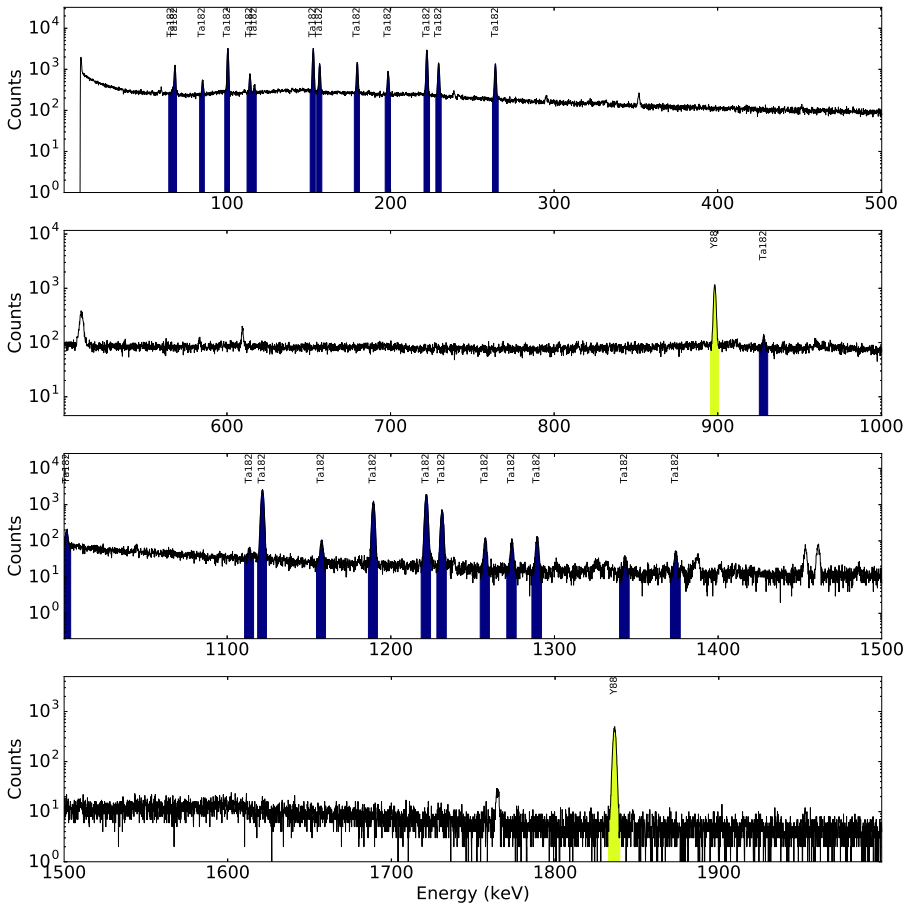

Figure 7: HPGe measurement taken from an Y foil 'YCCFE1', showing characteristic gamma lines from ^{88}Y and ^{182}Ta, the latter isotope being measured due to neutron activation of Ta impurities in the Y foil. The unmarked peaks are due to background environmental lines.

5. Comparisons of experimental measurements of activity against predicted values

A comparison of the calculated predictions of activity for each foil and isotope of interest, C, against the decay corrected experimental measurement, E, are shown in figures 8 to 18. The neutron yield data derived from the KN1 system are used to normalise the calculated neutron flux spectra determined from MCNP subsequently provided as input to calculations, to determine the 'C', performed using FISPACT-II (the reference activation code for ITER activation analyses) with the IRDFFv1.05 cross section library. The ^{58}Ni(n,n'p)^{57}Co dosimetry reaction does not exist in IRDFFv1.05, and in this case nuclear cross section data from the EAF-2010 and TENDL-2015 libraries have been used instead. The uncertainty in the KN1 neutron yield measurements used as input are approximately 10%. The uncertainties in the calculated reaction rates due to the uncertainties in the predicted neutron spectrum and the reaction cross-sections have been estimated using the RR_UNC code [22] and subsequently used in the FISPACT-II codes. The RR_UNC code reads neutron spectra, reaction cross-sections and associated covariance matrices, with covariance data from IRDFFv1.05, in ENDF-6 format [23] (Evaluated Nuclear Data Format).

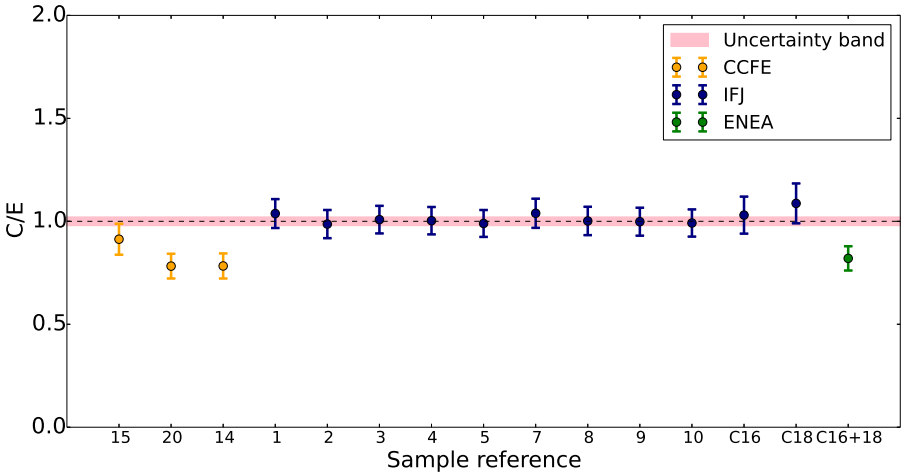

Figure 8: C/E plot for ^{nat}Ti(n,x)^{46}Sc. The '+' notation signifies that multiple foil samples measured together as a stack.

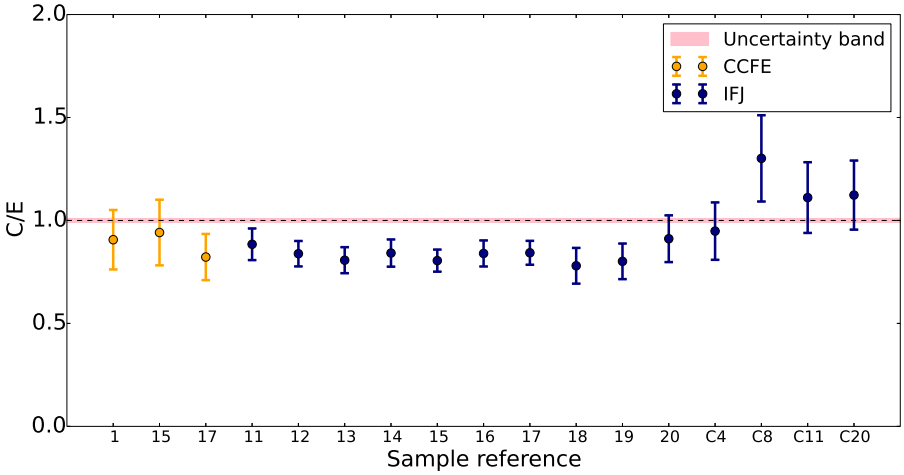

Figure 9: C/E plot for ^{nat}Ni(n,x)^{60}Co.

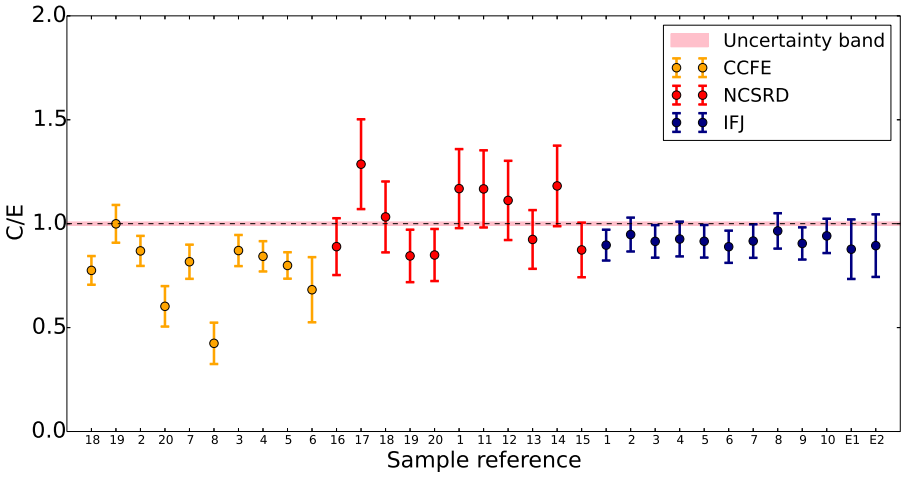

Figure 10: C/E plot for ^{59}Co(n,2n)^{58}Co.

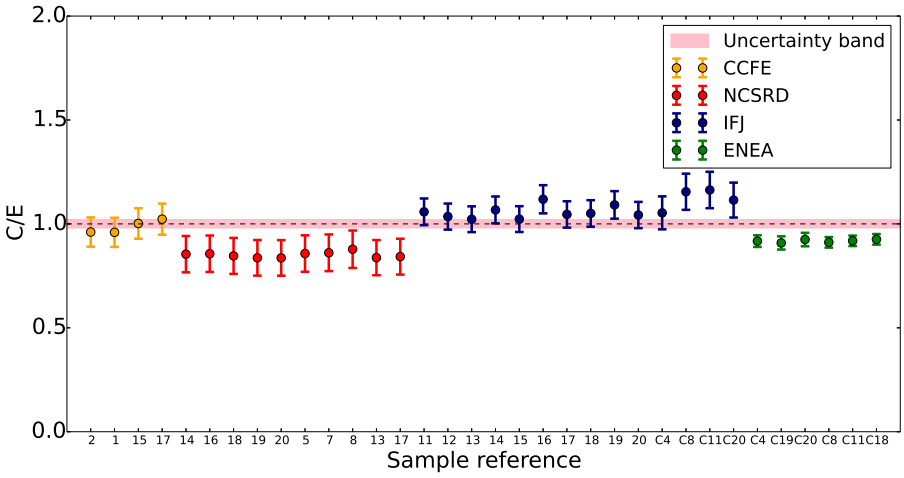

Figure 11: C/E plot for ^{nat}Ni(n,x)^{58}Co.

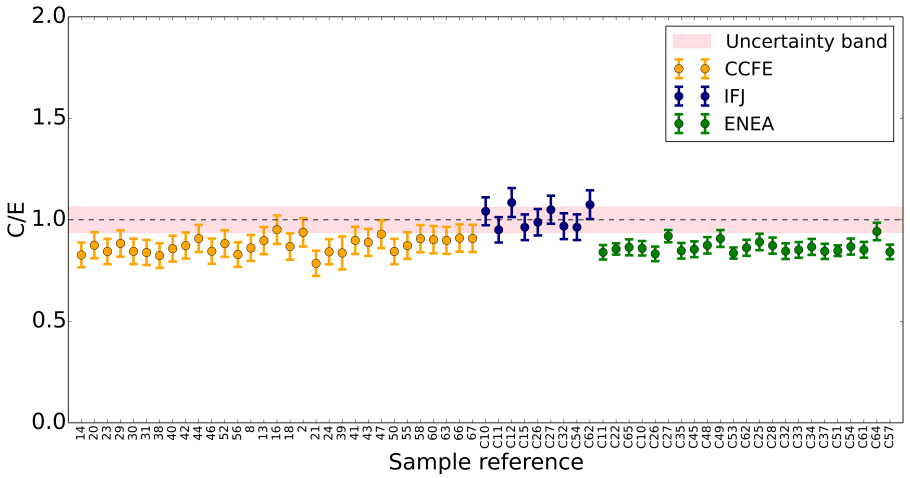

Figure 12: C/E plot for ^{nat}Fe(n,x)^{54}Mn.

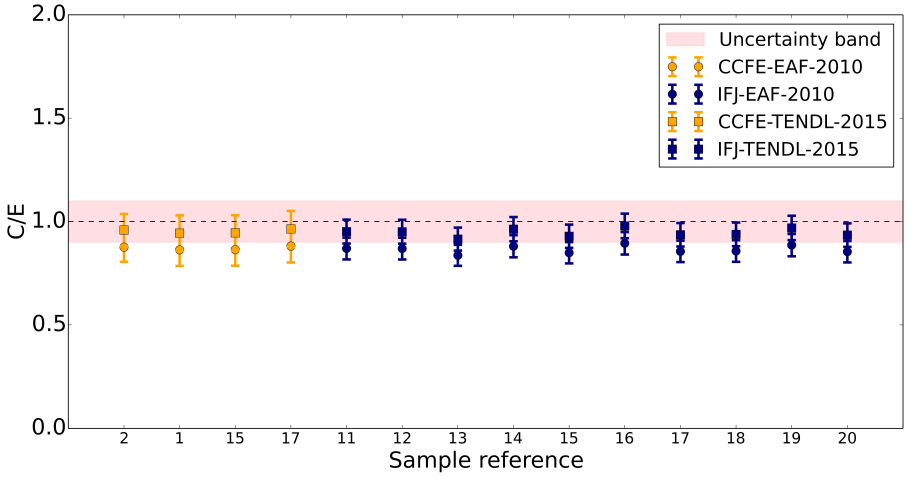

Figure 13: C/E plot for ^{nat}Ni(n,x)^{57}Co. Calculated values were performed using both EAF-2010 and TENDL-2015 in absence of IRDFFv1.05 data.

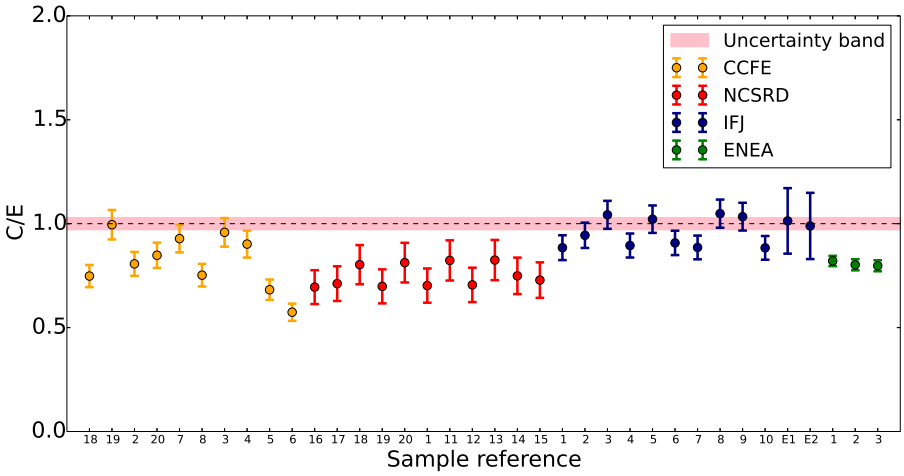

Figure 14: C/E plot for ^{59}Co(n,γ)^{60}Co.

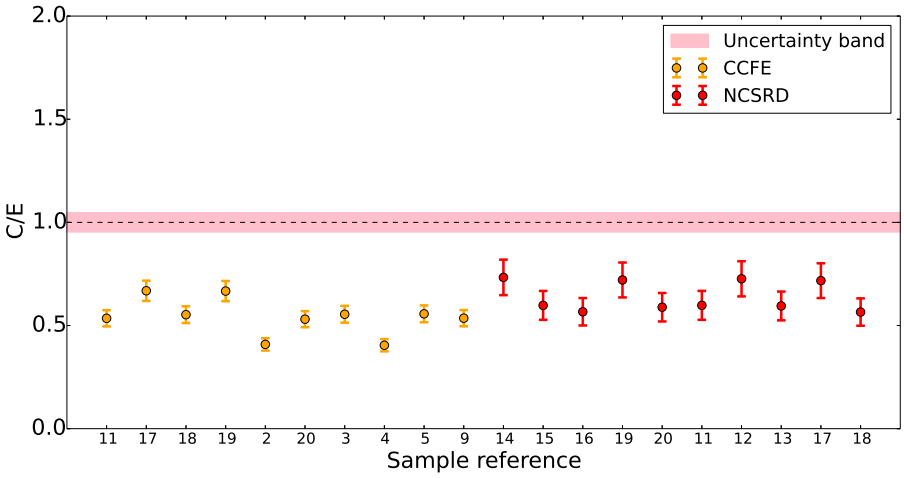

Figure 15: C/E plot for ^{181}Ta(n,γ)^{182}Ta.

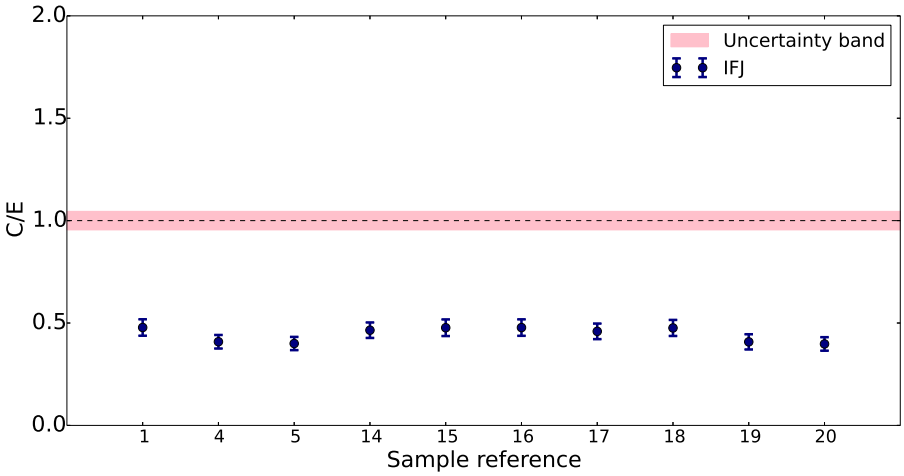

Figure 16: C/E plot for ^{45}Sc(n,γ)^{46}Sc.

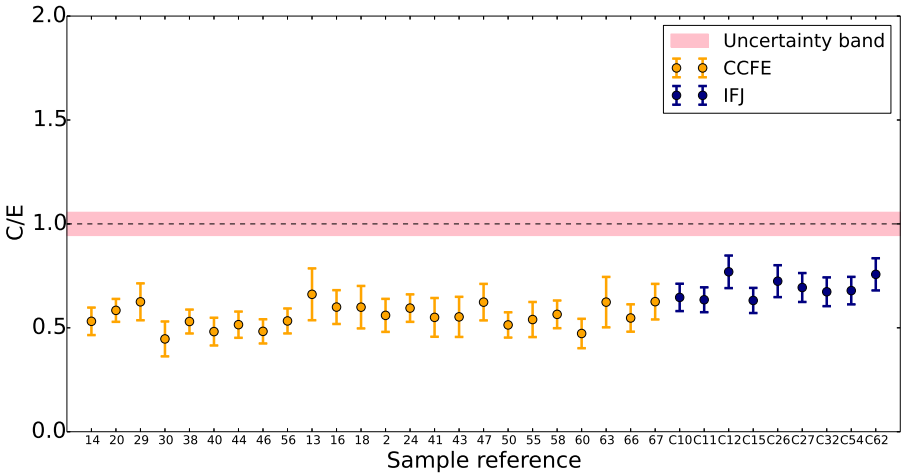

Figure 17: C/E plot for ^{58}Fe(n,γ)^{59}Fe.

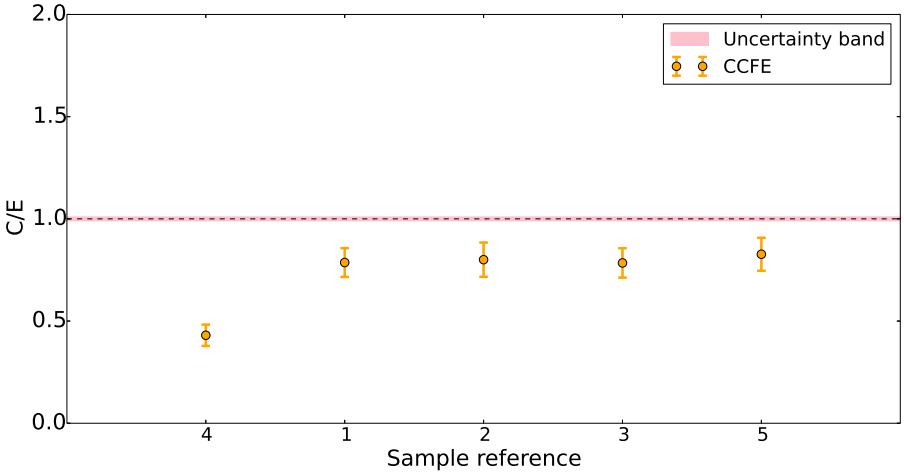

Figure 18: C/E plot for ^{89}Y(n,2n)^{88}Y.

6. Analysis and discussion of results

Characterisation experiments and supporting analyses for the long-term irradiation stations following JET experiments in 2015–16 have been completed. The level of agreement between experimentally measured dosimetry foil activities using four independent laboratories across six of the seven threshold reaction measurement data compared to those predicted via calculation gives a weighted average C/E (i.e. an average is taken where each individual C/E value is inversely weighted by its corresponding uncertainty) of 0.91 ± 0.01. Uncertainties relating to MCNP modeling geometry and material definition, nuclear cross section data and the reported neutron yield (by the KN1 fission counting system described earlier in the paper) are not included and could explain the remaining few percentage discrepancy. This, together with the apparent small systematic differences between groups of measurements at laboratories, particularly for the ^{nat}Ni(n,x)^{58}Co measurement (see figure 11), but also for the ^{nat}Ti(n,x)^{46}Sc reaction (see figure 8) will be investigated in future work. An inter-laboratory comparison activity between laboratories using ultra-high precision calibration sources is underway and planned to be completed in 2018, and may help to resolve small systematic differences, whilst simulation sensitivity analyses can be adopted as a strategy to determine modelling uncertainties.

The CCFE measurements of the seventh threshold reaction, ^{89}Y(n,2n)^{88}Y, exhibited a low weighted average C/E value of 0.67 ± 0.03. The ^{89}Y(n,2n)^{88}Y reaction has a high energy threshold—it is sensitive to D–T neutron energies, but not D–D energies, and thus its presence is a useful measure of the D–T contribution to the neutron spectrum. This particular set of measurements, with low C/E values, suggests that the assumed D–T contribution of 1%, used in the calculations is too high for the JET D–D campaign under study, and that the figure can be revised in future activities. Furthermore, in future JET campaigns the ^{89}Y(n,2n)^{88}Y reaction may be a useful measurement of the integrated 14 MeV neutron yield over the campaign, which may in principle be cross compared with a series of individual ^{93}Nb(n,2n)^{92m}Nb foil measurements

deployed per shot using the KN2 pneumatic transfer system. Such a measurement approach may be particularly useful to consider to complement the KN2 measurement system for a future T–T campaign, planned for 2019, which is also expected to produce a significant number of D–T neutrons from the presence of residual deuterium in JET wall materials which is expected to populate the plasma to some, as yet unknown, extent.

The comparison of C/E values for four capture reactions, ^{58}Fe(n,γ)^{59}Fe reaction (see figure 17), ^{45}Sc(n,γ)^{46}Sc reaction (see figure 16), ^{59}Co(n,γ)^{60}Co (see figure 14) and ^{181}Ta(n,γ)^{182}Ta (see figure 15) reactions all exhibit low C/E, with a weighted average C/E value across the four sets of measurements of 0.66 ± 0.01, suggesting that the thermal neutron flux is under-predicted in the calculated results. The C/E plot for the ^{59}Co(n,γ)^{60}Co and ^{181}Ta(n,γ)^{182}Ta reactions show a larger spread of values across the four laboratories overall, 30% in particular cases. In addition, for these capture reactions there is a greater spread across individual measurements, suggesting that local neutronics effects specific to foil positions and ordering may need to be modelled in more detail in order to obtain improved agreement. The LTIS MCNP model that was used in this work used geometry representing single foils of Co, Sc, Ta and Fe (each specific foil was not modeled exactly in every location) in order to determine representative neutron capture reaction rates in these four cases. The corresponding reaction rates were determined using pointwise cross-section data using the IRDFF-1.05 library within MCNP to account for resonance self shielding effects. This is in contrast to the approach taken with threshold reactions, where self-shielding is not relevant, and in these cases reaction rates were determined using the method of collapsing a group-wise nuclear data library with a group-wise neutron spectrum. Figure 19 shows an example pointwise cross section comparison of EAF-2010, IRDFF-1.05, TENDL-2015 and EXFOR measurements for the ^{59}Co(n,γ)^{60}Co reaction, exhibiting several resonances, including a giant resonance at 132 eV, and a characteristic 1/v region at energies below this resonance. Co foils with a thickness of 0.5 mm and some with 0.05 mm thickness were irradiated in these experiments. Three of the ENEA foil

samples were performed at the IFJPAN laboratory (see points labelled 1, 2 and 3 under the 'ENEA' grouping in figure 14) and were conducted using the thinner Co foils. Since self-shielding effects are particularly important for the ^{59}Co(n,γ)^{60}Co reaction, due to the giant resonance in particular, the relevant reaction rates were calculated individually for the specific foil thickness using the pointwise MCNP calculations with the IRDFF-1.05 library.

7. Conclusions

In summary, these activation experiments and supporting calculations show that our models and the simulation approach taken is able to predict, currently to better than 10%, the levels of activity resulting from a range of threshold reactions in a complex fusion environment and operational scenario. The calculation scheme represents an integrated test of the geometric and materials representations within the JET and LTIS assembly MCNP model that has been developed, the FISPACT-II code and corresponding nuclear data libraries, and the reporting of neutron yield via the KN1 system over 3682 experimental shots. The methodology adopted and demonstrated in this work may also be useful if deployed in an inverse sense i.e. to be used as a practical way to perform absolute measurements of neutron fluence for JET, and ultimately for ITER, with the caveat that a reliable and well-defined radiation transport model containing appropriate geometry and material composition would be a necessity. The work has also highlighted that improvements in modelling detail are still necessary for the JET MCNP model used in this activity to improve agreement between simulation and experiment for capture reaction rates. This improved modelling strategy will be adopted in future work to capture local spatial effects, i.e. those that impact on the low energy part of the neutron spectrum, which have been shown to be important to improve the predictions of capture reactions.

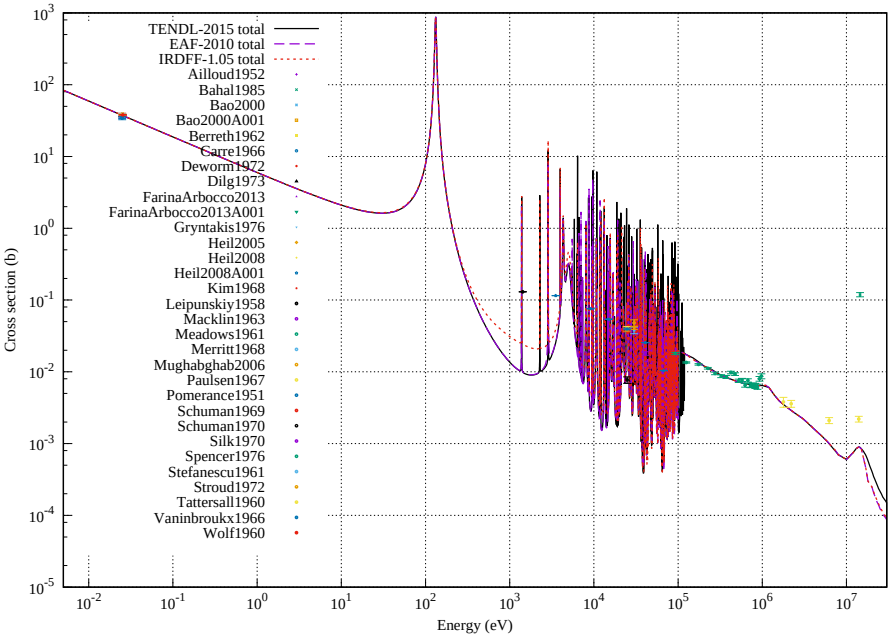

Figure 19: Cross section comparisons of EAF-2010, IRDFF-1.05, TENDL-2015 and EXFOR measurements for the ^{59}Co(n,γ)^{60}Co reaction.

8. Acknowledgements

This work has been carried out within the framework of the EUROfusion Consortium and has received funding from the Euratom research and training programme 2014-2018 under grant agreement No 633053 and from the RCUK Energy Programme [grant number EP/P012450/1]. The views and opinions expressed herein do not necessarily reflect those of the European Commission.

References

[1] P. Batistoni, D. Campling, S. Conroy, D. Croft, T. Giegerich, T. Huddleston, X. Lefebvre, I. Lengar, S. Lilley, A. Peacock, M. Pillon, S. Popovichev, S. Reynolds, R. Vila, R. Villari, N. Bekris, Technological exploitation of Deuterium-Tritium operations at JET in support of ITER design, operation and safety, Fusion Engineering and Design 109 (Part A) (2016) 278 – 285, proceedings of the 12th International Symposium on Fusion Nuclear Technology-12 (ISFNT-12). doi:https://doi.org/10.1016/j.fusengdes.2016.03.012.

[2] X. Litaudon et al, Overview of the JET results in support to ITER, Nuclear Fusion 57 (10) (2017) 102001.

[3] P. Batistoni, On the absolute calibration of neutron measurements in fusion reactors, Fusion Engineering and Design 105 (Supplement C) (2016) 58 – 69. doi:https://doi.org/10.1016/j.fusengdes.2016.02.064.
URL http://www.sciencedirect.com/science/article/pii/S0920379616301466

[4] R. Villari, P. Batistoni, M. Angelone, J. Catalan, B. Colling, D. Croft, U. Fischer, D. Flammini, A. Klix, S. Loreti, S. Lilley, F. Moro, J. Naish, L. Packer, P. Pereslavtsev, S. Popovichev, P. Sauvan, B. Syme, Neutronics experiments and analyses in preparation of DT operations at JET, Fusion Engineering and Design 109 (Part A) (2016) 895 – 905, proceedings of the

12th International Symposium on Fusion Nuclear Technology-12 (ISFNT-12). doi:https://doi.org/10.1016/j.fusengdes.2016.01.055.
URL http://www.sciencedirect.com/science/article/pii/S0920379616300576

[5] R. Villari, P. Batistoni, J. Catalan, B. Colling, D. Croft, U. Fischer, D. Flammini, N. Fonnesu, L. Jones, A. Klix, B. Kos, M. K?osowski, I. Kodeli, S. Loreti, F. Moro, J. Naish, B. Obryk, L. Packer, P. Pereslavtsev, R. Pilotti, S. Popovichev, P. Sauvan, I. Stamatelatos, T. Vasilopoulou, ITER oriented neutronics benchmark experiments on neutron streaming and shutdown dose rate at JET, Fusion Engineering and Designdoi:https://doi.org/10.1016/j.fusengdes.2017.03.037.
URL http://www.sciencedirect.com/science/article/pii/S0920379617302405

[6] B. Obryk, P. Batistoni, S. Conroy, B. D. Syme, S. Popovichev, I. E. Stamatelatos, T. Vasilopoulou, P. Bilski, Thermoluminescence measurements of neutron streaming through JET Torus Hall ducts, Fusion Engineering and Design 89 (9) (2014) 2235 – 2240, proceedings of the 11th International Symposium on Fusion Nuclear Technology-11 (ISFNT-11) Barcelona, Spain, 15-20 September, 2013. doi:https://doi.org/10.1016/j.fusengdes.2013.12.045.

[7] P. Batistoni, S. Conroy, S. Lilley, J. Naish, B. Obryk, S. Popovichev, I. Stamatelatos, B. Syme, T. Vasilopoulou, J. contributors, Benchmark experiments on neutron streaming through JET Torus Hall penetrations, Nuclear Fusion 55 (5) (2015) 053028.

[8] T. Vasilopoulou, I. Stamatelatos, P. Batistoni, S. Conroy, B. Obryk, S. Popovichev, D. Syme, Neutron streaming along ducts and labyrinths at the JET biological shielding: Effect of concrete composition, Radiation Physics and Chemistry 116 (Supplement C) (2015) 359 – 364, proceedings of the 9th International Topical Meeting on Industrial Radiation and Ra-

dioisotope Measurement Applications. doi:https://doi.org/10.1016/j.radphyschem.2015.04.015.

[9] B. C. Colling et al., Testing of tritium breeder blanket activation foil spectrometer during JET operations, Fusion Engineering and Design - article in press.

[10] L. Packer, P. Batistoni, B. Colling, K. Drozdowicz, S. Jednorog, M. Gilbert, E. Laszynska, D. Leichtle, J. Mietelski, M. Pillon, I. Stamatelatos, T. Vasilopoulou, A. Wjcik-Gargula, Status of ITER material activation experiments at JET, Fusion Engineering and Designdoi:https://doi.org/10.1016/j.fusengdes.2017.01.037.

[11] G. Stankunas, A. Tidikas, P. Batistoni, I. Lengar, Analysis of activation and damage of ITER material samples expected from DD/DT campaign at JET, Fusion Engineering and Designdoi:https://doi.org/10.1016/j.fusengdes.2017.07.013.

[12] X-5 Monte Carlo Team, MCNP – a general purpose Monte Carlo N-Particle transport code, version 5, volume II: User's guide, los Alamos document number: LA-CP-03-0245. (2008 revision).

[13] Y. Wu, CAD-based interface programs for fusion neutron transport simulation, Fusion Engineering and Design 84 (7) (2009) 1987 – 1992, proceeding of the 25th Symposium on Fusion Technology. doi:https://doi.org/10.1016/j.fusengdes.2008.12.041.

[14] J.-C. Sublet, J. Eastwood, J. Morgan, M. Gilbert, M. Fleming, W. Arter, FISPACT-II: An Advanced Simulation System for Activation, Transmutation and Material Modelling, Nuclear Data Sheets 139 (Supplement C) (2017) 77 – 137, special Issue on Nuclear Reaction Data. doi:https://doi.org/10.1016/j.nds.2017.01.002.

[15] P. Batistoni et al., 14 MeV Calibration of JET neutron detectors Phase

1: calibration and characterization of the neutron source, Nuclear Fusion - article in press xx (xx) (2018) xx.

[16] S. Conroy, O. Jarvis, G. Sadler, G. Huxtable, Time resolved measurements of triton burnup in JET plasmas, Nuclear Fusion 28 (12) (1988) 2127. URL http://stacks.iop.org/0029-5515/28/i=12/a=001

[17] O. N. Jarvis, S. Conroy, Prediction/modelling of the neutron emission from JET discharges, Plasma Physics and Controlled Fusion 44 (8) (2002) 1651. URL http://stacks.iop.org/0741-3335/44/i=8/a=316

[18] Update of X Ray and Gamma Ray Decay Data Standards for Detector Calibration and Other Applications, Tech. Rep. Vol 1, IAEA (2007).

[19] Brookhaven National Laboratory, Tech. Rep. BNL chart of the nuclides, BNL.

[20] S. Sudar, TRUECOINC Version 1.01a, A program for calculation of true coincidence corrections for gamma rays.

[21] ISOCS/LabSOCS Detector Efficiency Characterization, further details at http://canberra.com/products/radiochemistry_lab/isocs-characterization.asp/.

[22] Andrej Trkov, private communication.
URL https://www-nds.iaea.org/IRDFF/rr_unc.for

[23] CSEWG Members, ENDF-6 Formats Manual, Data Formats and Procedures for the Evaluated Nuclear Data Files, ENDF/B-VI and ENDF/B-VII, CSEWG Document ENDF-102, Report BNL-90365-2009, Rev.2, SVN Commit: Revision 85, 2012.